Journal of Luminescence 171 (2016) 246–253

Contents lists available at ScienceDirect

Journal of Luminescence

journal homepage: www.elsevier.com/locate/jlumin

Full Length Article

Temperature dependent luminescence Cr^{3+}-doped $GdAl_3(BO_3)_4$ and $YAl_3(BO_3)_4$

Beata Malysa [a], Andries Meijerink [b,*], Thomas Jüstel [a,**]

[a] Münster University of Applied Sciences, Stegerwaldstrasse 39, 48565 Steinfurt, Germany
[b] University Utrecht, Princetonplein 1, NL-3584 Utrecht, The Netherlands

ARTICLE INFO

Article history:
Received 15 June 2015
Received in revised form
16 October 2015
Accepted 19 October 2015
Available online 24 November 2015

Keywords:
Trivalent chromium
Thermal quenching
Photoluminescence
Near infrared phosphors
Huntite-type borates

ABSTRACT

Chromium activated $YAl_3(BO_3)_4$ (YAB) and $GdAl_3(BO_3)_4$ (GAB) were synthesized and show efficient broad band near infrared emission under excitation in the UV, blue and orange spectral regions. Temperature dependent luminescence measurements for GAB:1%Cr^{3+} and YAB:1%Cr^{3+} reveal high quenching temperatures for the broad band Cr^{3+} emission, 620 K for YAB:Cr and 650 K for GAB:Cr. To gain insight in the luminescence the crystal field strength, Racah parameters, nephelauxetic effect and phonon coupling parameters have been investigated by using spectroscopic data. The crystal field splitting for Cr^{3+} is similar in the two borates (around 1670 cm^{-1}). However, the calculated B Racah parameters indicate a higher global covalency in GAB. The electron phonon-coupling parameter (S) and the effective phonon energy ($\hbar\omega$) were determined to be 5.9 and 263 cm^{-1} for YAB and 5.4 and 309 cm^{-1} for GAB, respectively. The larger electron–phonon coupling strength in YAB:Cr is in agreement with the lower quenching temperature in comparison with GAB:Cr.

1. Introduction

The transition metal ion Cr^{3+} is widely applied in solid state laser gain materials, as a co-dopant for persistent phosphors emitting in the NIR, and as the optical centre in thermographic phosphors for optical sensing [1–6]. Moreover, Cr^{3+} doped luminophores are also considered as near infrared (NIR) emitting materials for in-vivo optical imaging due to the rather high penetration depth of NIR radiation into human tissue [7,8]. Just as in the field of lighting, the availability of efficient and high power blue LEDs enables the manufacturing of energy efficient and high power NIR sources by pumping an NIR phosphor with by a blue or near ultraviolet (NUV) emitting (In,Ga)N diode. Spectral conversion from blue/NUV to NIR involves a significant energy dissipation, more than for blue/NUV to visible conversion. This means that the radiation converter should not suffer from thermal quenching up to about 450 K, a temperature that may even exceeded if the converter is in intimate contact to the die [9,10].

The borate hosts $YAl_3(BO_3)_4$ and $GdAl_3(BO_3)_4$ are known for their good chemical and thermal stability [11,12]. Moreover, Cr^{3+} doped YAB and GAB show efficient NIR photoluminescence upon excitation by NUV and blue light [13]. Here we will investigate the optical properties of both Cr-doped borates and evaluate their potential as NIR emitter for application in high power broad band NIR sources. To this end, both low temperature studies (down to 4 K) are performed to provide understanding of the energy level structure underlying the optical properties as well as high temperature measurements to study the thermal quenching and the temperature dependence of the photoluminescence spectra of YAB:Cr and GAB:Cr up to 800 K.

2. Experimental section

2.1. Synthesis

$YAl_3(BO_3)_4$ and $GdAl_3(BO_3)_4$ doped with Cr^{3+} ions were synthesized by conventional solid state reaction in air atmosphere. As starting materials Al_2O_3 (VWR-Prolabo, 99.99%), Cr_2O_3 (Alfa Aesar, 99.95%), Y_2O_3 (Treibacher, 99.95%), Gd_2O_3 (Treibacher, 99.90%), H_3BO_3 (Merck, 99.95%), were used. An excess of H_3BO_3 was added in order to compensate its evaporation during the calcination process. The starting materials were mixed and ground in an agate mortar. Then, the powders were pre-calcinated at 500 °C for 2 h and finally sintered at 1100 °C for 4 h.

* Corresponding author. Tel.: +31 302532202.
** Corresponding author. Tel.: +49 2551962205.
E-mail addresses: beata.malysa@fh-muenster.de (B. Malysa), a.meijerink@uu.nl (A. Meijerink), tj@fh-muenster.de (T. Jüstel).

http://dx.doi.org/10.1016/j.jlumin.2015.10.042
0022-2313/

2.2. Characterization

The X-ray diffraction patterns were measured on a Rigaku MiniFlex II diffractometer. As a radiation source a copper X-ray tube with Cu Kα radiation with 1.54 Å wavelength was used. The samples were examined in the region of 2θ between 10° and 80° with a scanning rate 10° per min.

Excitation and emission spectra were recorded on an Edinburgh Instruments FSL 920 spectrometer equipped with a 450 W Xe arc lamp, mirror optics for powder samples and a cooled (−20 °C) single-photon counting photomultiplier from Hamamatsu (R2658P). The correction file for the emission spectra was obtained from a tungsten incandescent lamp certified by NPL (National Physics Laboratory, UK). Diffuse reflection spectra were recorded on an Edinburgh Instruments FS900 spectrometer equipped with a 450 W Xe arc lamp and a cooled single-photon counting photomultiplier (Hamamatsu R928). $BaSO_4$ (99.99%, Sigma-Aldrich) was used as a reflectance standard. Luminescence decay curves were measured with a fluorescence spectrometer FLS920 (Edinburgh Instruments) with a Xe-μs-flash lamp also with the R2658P single-photon counting photomultiplier tube (Hamamatsu) in the mirror optic.

For recording thermal quenching (TQ) curves a cryostat "MicrostatN" from Oxford Instruments was introduced in the above described spectrometer equipment. Measurements were carried out from 77 to 500 K in 50 K steps. For TQ measurements in the range from 350 to 800 K an in-house constructed sample holder was used. This holder comprises a heater located underneath the cavity for the sample and is made of corundum ceramic. The heater comprises an ISA®-CHROM60 filament with a diameter of 0.5 mm. The housing of the sample holder was actively cooled by flowing water.

3. Results and discussion

3.1. Description of the crystal structure of the GAB and YAB host materials

The crystal type $RX(BO_3)_4$, where $R=Y^{3+}$ or Gd^{3+} and $X=Al^{3+}$ belongs to a group of double borates which have a huntite $[CaMg_3(CO_3)_4]$ structure with trigonal crystal system in the R32 space group (Fig. 1)[14,15].

In this system, Y^{3+} and Gd^{3+} ions occupy nearly regular trigonal prismatic sites. Al^{3+} ions reside in distorted octahedral sites and boron is arranged in sheets of BO_3^{3-} triangles. Gd^{3+} (Y^{3+}) ions are separated from each other by the borate groups and do not share the same oxygen ion. Hence, the distance between the nearest Gd^{3+}–Gd^{3+} and Y^{3+}–Y^{3+} neighbor ions is large and equals 5.895 Å and 5.883 Å, respectively [16]. It allows a higher doping level of trivalent rare earth metal ions without concentration quenching. A shorter distance between the nearest neighbor ions causes a higher probability of the non-radiative energy transfer from one ion to another which leads to concentration quenching because of energy migration to quenching centers [17].

Cr^{3+} ions have a strong preference for octahedral coordination because of a high crystal field stabilization energy. Additionally, Cr^{3+} ions favor substitution on the octahedral Al^{3+} site because of the similarity of crystal ionic radius: Al^{3+} (67.5 pm), Cr^{3+} (75.5 pm) [18] and identical charges of both ions (no charge compensation is required) [19,20]. The ionic radii of Y^{3+} and Gd^{3+} ions in 6-fold coordination are 104 pm and 108 pm, respectively. Hence, it is unlikely that Cr^{3+} ions replace Y^{3+} due to the large difference in ionic radii.

Moreover, YAB and GAB host materials are excellent for Cr(III)-substitution because they offer only one kind of cation site with octahedral coordination. Host lattices which have both 6-fold coordinated and 4-fold coordinated Al^{3+} sites gives rise to the incorporation of Cr^{6+} [21]. The presence of chromate anions $[CrO_4]^{2-}$ strongly reduces the luminescence efficiency, even in low concentrations because of the strong charge transfer absorption band in the visible spectral region. In the presently investigated borates chromate formation is prevented.

In order to compare the influence of the host material on the Cr^{3+} luminescence spectra, it is important to consider the distances between Al^{3+} ion and O^{2-} ligands (Fig. 1). The value of the crystal field splitting is inversely proportional to the distance between cation and ligands (R) as given by the relation $10Dq \sim (1/R^5)$ [22]. It indicates that even a small change in the length of any metal–ligand bond considerably alters the crystal field splitting. By comparison the lengths of the Al–O bonds in YAB and GAB structures (Table 1), we predict a larger splitting of the energy of the 3d orbitals for Cr^{3+} substitution on Al^{3+} sites in YAB.

3.2. Phase formation

Crystal structure and the phase purity of GAB:1%Cr^{3+} and YAB:1%Cr^{3+} phosphors were examined by recording X-ray diffraction patterns and are plotted in Fig. 2. The positions and

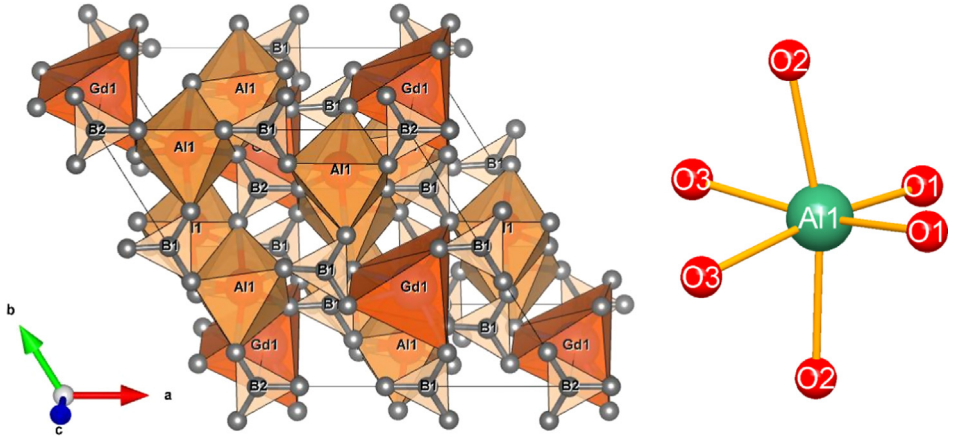

Fig. 1. Illustration of the crystal structure of $GdAl_3(BO_3)_4$ (on the left) and a view of the $[AlO_6]^{9-}$ unit (on the right).

Table 1
Distance between central metal ion (Al^{3+}) and ligands (O^{2-}) in the GAB and YAB compounds.

Kind of bond	GAB (Å)	YAB (Å)
Al–O1	1.954	1.948
Al–O2	2.025	2.018
Al–O3	2.024	2.018

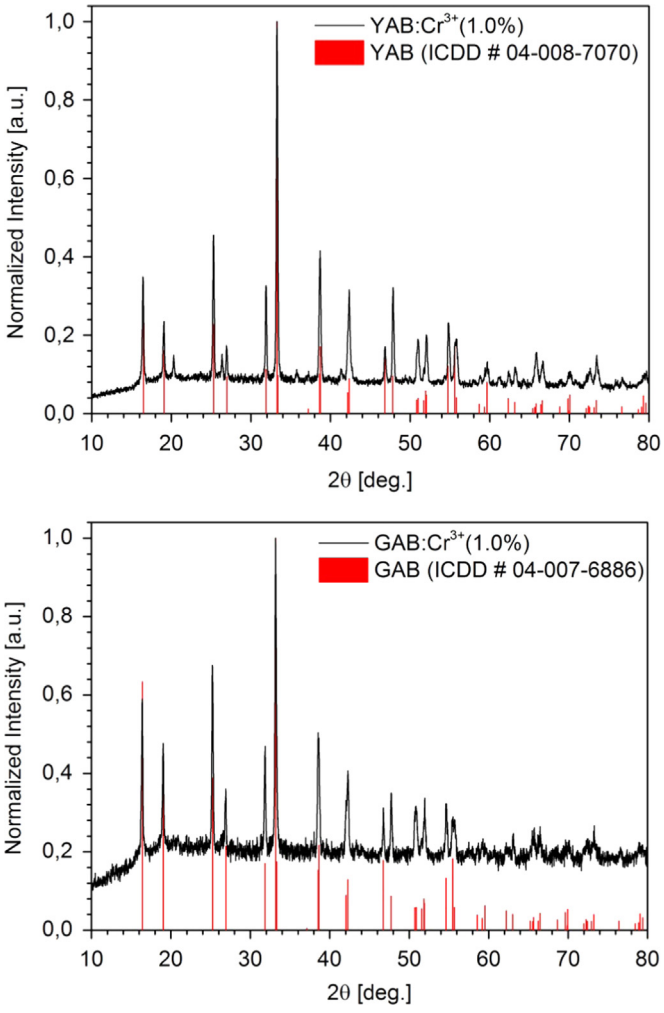

Fig. 2. Powders XRD patterns of $Y(Al_{1-x}Cr_x)_3(BO_3)_4$ and $Gd(Al_{1-x}Cr_x)_3(BO_3)_4$, where $x=0.01$.

relative intensities of the observed XRD peaks are in good agreement with standard data (ICDD 04-008-7070 for YAB and ICDD04-007-6886 for GAB). The samples are single phase. It indicates that 1% of Cr^{3+} ions do not change the crystal structure of YAB and GAB, as can be expected.

The XRD patterns exhibit a small shift of the refraction peaks towards higher 2θ values in relation to the undoped host materials because of a small increase of the lattice parameters. The unit cell of the host becomes slightly larger as a consequence of the Cr-substitution on the Al-site, consistent with the larger ionic radius of Cr^{3+} [23].

In the XRD graph of GAB:1%Cr^{3+} a characteristic background noise is observed. The origin of this background can occur as a result of the fluorescence radiation by cause of the interaction of samples with the high energy photons emitted from an X-ray source [24]. The noticeable signal can be ascribed to the gadolinium fluorescence during XRD measurements [25,26].

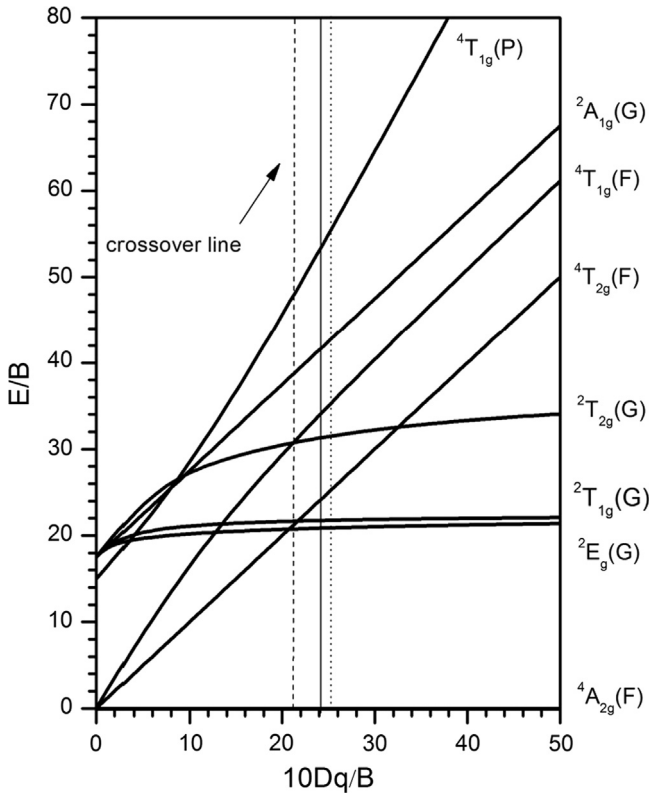

Fig. 3. Tanabe-Sugano diagram for the d^3 electronic configuration in octahedral symmetry. The 10Dq/*B* values of YAB:1%Cr (solid line) and GAB:1%Cr (dotted line) are indicated.

3.3. Optical properties at room temperature

3.3.1. Tanabe Sugano diagram

Cr^{3+} has a $[Ar]3d^3$ electronic configuration and its optical spectra can be interpreted on the basis of the Tanabe-Sugano diagram for d^3 ions in octahedral coordination (Fig. 3) [27]. Depending on the crystal field strength, the lowest Cr^{3+} emitting levels can be either $^4T_{2g}$ or ^2E_g. For a strong crystal field systems, the lowest excited state is ^2E_g which is identified with a narrow R-line emission arising from the spin-forbidden transition $^2E_g \rightarrow {}^4A_{2g}$. For weak crystal field systems, the lowest excited state is $^4T_{2g}$. The spin-allowed transition $^4T_{2g} \rightarrow {}^4A_{2g}$ is characterized by a strong coupling to the lattice causing a broad emission band [28]. The interaction with lattice vibrations is stronger for the $^4A_2$ (t_{2g}^3) to $^4T_{2g}$ ($t_{2g}^2 e_g$) transition than for the transition to the ^2E_g (t_{2g}^3) state. The quartet $^4T_{2g}$ state involves an occupation of the e_g orbital which changes the bonding with the ligand ions. Hence, the transition to the $^4T_{2g}$ excited state is strongly affected by host vibrations [29].

3.3.2. Emission, excitation and reflection spectra at room temperature

Fig. 4a and b display emission, excitation and reflection spectra of YAB:1%Cr^{3+} and GAB:1%Cr^{3+}, respectively. As can be observed both materials reveal broad absorption and excitation bands located in the blue (near 425 nm) and orange (near 600 nm) spectral range which are characteristic for Cr^{3+} ions and can be attributed to the spin-allowed electronic transition from the ground state $^4A_{2g}(^4F)$ to the excited states $^4T_{1g}(^4F)$ and $^4T_{2g}(^4F)$, respectively. The higher energy bands with a maximum around 265 nm corresponds to the $^4A_{2g}(^4F) \rightarrow {}^4T_{1g}(^4P)$ transition [30]. For GAB:1%Cr^{3+} several narrow peaks are observed which can be assigned to transitions of Gd^{3+} ion. The most intensive sharp

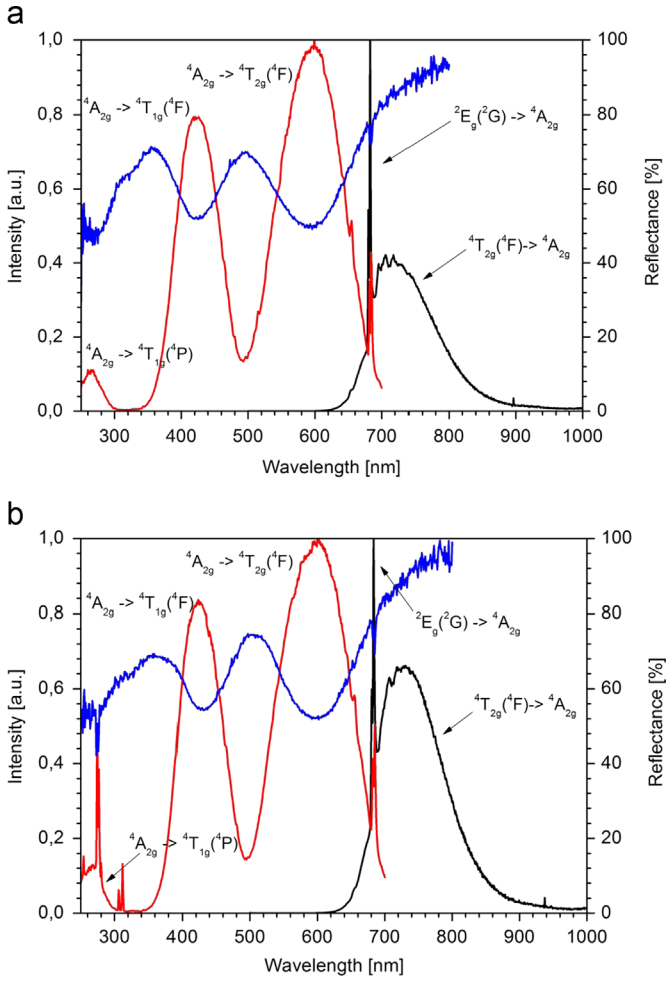

Fig. 4. Emission (black line), excitation (red line) and reflection spectra (blue line) of (a) YAB:1%Cr^{3+} and (b) GAB:1%Cr^{3+} phosphors at room temperature. Emission spectra are recorded for excitation at 420 nm and excitation spectra are recorded for 720 nm emission. (For interpretation of the references to color in this figure legend, the reader is referred to the web version of this article.)

peaks around 275 and 310 nm are due to the electronic transitions $^8S_{7/2}\rightarrow{}^6I_J$ and $^8S_{7/2}\rightarrow{}^6P_J$, respectively [16]. As can be observed, Cr^{3+} ions show a broad absorption band in the range where Gd^{3+} emits (~310 nm) and explains that Gd^{3+} can act as a sensitizer for Cr^{3+} emission in GAB:Cr^{3+}. Besides, in the excitation spectra some weak and narrow peaks at 655 and 680 nm are observed which can be assigned to the spin-forbidden transitions between the ground state $^4A_{2g}(^4F)$ and the excited states $^2T_{1g}(^2G)$ and $^2E_g(^2G)$, respectively [31].

The emission spectra of YAB:1%Cr^{3+} (Fig. 4a) and GAB:1%Cr^{3+} (Fig. 4b) were recorded for excitation at 420 nm. Both Cr-phosphors emit in the NIR range. The room temperature emission spectra extend from 600 to 900 nm and consist of both narrow line emission around 680 nm and a broad band with a maximum at 720 nm for YAB:Cr^{3+} and 733 nm for GAB:Cr^{3+}. The narrow line emission is assigned to the $^2E_g\rightarrow{}^4A_{2g}$ transition and the broad band to the $^4T_{2g}\rightarrow{}^4A_{2g}$ transition, consistent with emission for Cr^{3+} in intermediate crystal field materials. The ratio 10 Dq/B is situated just on the right side of the cross-overline in the Tanabe-Sugano diagram (Fig. 3). At room temperature thermal population of the $^4T_{2g}$ level occurs and emission is observed from both the ^2E_g and $^4T_{2g}$ states in thermal equilibrium which is usually identified as the situation for an intermediate crystal field splitting [7,20].

Table 2
Crystal field strength, Racah parameters and β-covalency of YAB:1%Cr and GAB:1% Cr determined from the energy values at the peaks of the $^4A_{2g}\rightarrow{}^4T_{2g}$ and $^4A_{2g}\rightarrow{}^4T_{1g}$ transitions as determined from the absorption spectra. Emission maxima are determined from the room temperature emission spectra.

Parameter	YAB:Cr	GAB:Cr
$E(^2E_g)$ [cm^{-1}]	14,652	14,630
$E(^4T_{2g})$ [cm^{-1}]	16,750	16,722
$E(^4T_{1g})$ [cm^{-1}]	23,640	23,474
B [cm^{-1}]	695	677
C [cm^{-1}]	2828	2877
10 Dq [cm^{-1}]	16,750	16,722
Dq/B	2.40	2.47
$\beta=B/B_0$	0.70	0.68
E_{em} ($^4T_2$) [cm^{-1}]	13,889	13,643

3.3.3. *Crystal field strength, Racah parameters, β-covalency values*

As 3d electrons of the transition metal ions are not shielded from their surroundings by outer filled shells, the optical properties of Cr^{3+} are rather sensitive to the environment. The influence of the host lattice on the Cr^{3+} spectra is expressed by spectroscopic parameters such as the crystal field splitting (10Dq), the B and C Racah parameters. The nephelauxetic effect reduces the Racah parameters relative to the free ion values and is expresses by β (B/B_0, where B_0 is the free ion value). The nephelauxetic effect is related to the covalency of Cr^{3+} to ligand bonding and a higher covalency reduces β. The values for 10 Dq, B and C can be determined from the position of the excitation and emission bands [32,33]. The parameters were calculated from the energy values at the peaks of the $^4A_{2g}\rightarrow{}^4T_{2g}$ and $^4A_{2g}\rightarrow{}^4T_{1g}$ transitions and are collected in Table 2. The parameters differ slightly from those determined by Wang et al. [14,33]. Especially, the lower energy position for the $^4T_2$ absorption band for Cr^{3+} in YAB compared to GAB is different from the present results. Close inspection of the spectra reported in Ref. [33] suggests that also here the $^4T_2$ band in YAB:Cr^{3+} is at a slightly higher energy but due to the high sloping background, an accurate determination of the position is difficult. In the present spectra, possibly due to the lower Cr^{3+} concentration, the background absorption is lower allowing a more accurate determination of the absorption band maxima.

The value determined for Dq is higher for Cr^{3+} in YAB consistent with the smaller distances between Al^{3+} and oxygen ligands in YAB compared to GAB (Table 1). B and C Racah parameters of the free Cr^{3+} ion equal 918 cm^{-1} and 3850 cm^{-1}, respectively [34]. The incorporation of Cr^{3+} ions into different host materials causes a decrease of the interelectronic repulsion parameters due to covalent bonding. The lower value of B Racah parameter (677 cm^{-1}) for GAB in comparison with YAB (B=695 cm^{-1}) indicates on the higher degree of the covalency in GAB. Trueba et al. [35] have recently reported that the values of 10Dq and Racah parameters show a different sensitivity to the metal–ligand distance. They found that Racah parameters are almost independent on the distance between metal and ligands but reveal a stronger dependence on the host covalency while the 10Dq value strongly depends on the local covalency between metal and ligands. As a result, the crystal field splitting exhibits a higher sensitivity to the metal–ligand distance (Cr^{3+}–O^{2-}) in comparison to the Racah parameters. The lower value for B in GAB indicates that the overall covalency of the host is larger in GAB than in YAB which is consistent with the smaller ionic radius of Y^{3+} vs. Gd^{3+}. Highly charged smaller cations give rise to more ionic bonding, reducing the covalency.

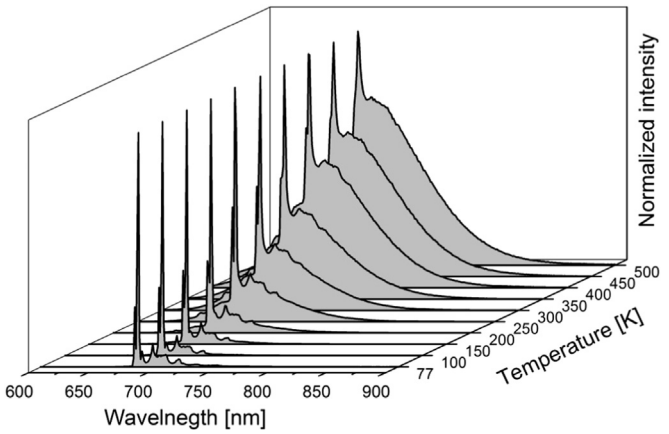

Fig. 5. Temperature dependent emission spectra of YAB:1%Cr phosphor upon excitation at 420 nm.

4. Temperature dependent luminescence

The values of Dq/*B* for YAB and GAB are 2.40 and 2.47, respectively. YAB:Cr^{3+} and GAB:Cr^{3+} show both narrow and broad band emission at room temperature (Fig. 4) and therefore we classify the situation for these materials as intermediate crystal field strengths (Dq/B values are near the crossover point ~2.2) [28]. In such a system, the energy between the two excited states ^2E_g and $^4T_{2g}$ is small and the long lived ^2E_g state can be considered as an energy level that acts as a reservoir for the higher lying $^4T_{2g}$ energy level. At low temperatures only ^2E_g emission is observed but upon raising the temperature a thermal equilibrium between the doublet and quartet levels occurs and both ^2E_g line emission and $^4T_{2g}$ band emission are observed. Since the emission occurs from two levels in thermal equilibrium, the lifetime for the line and broad band emission is expected to be the same [36]. At higher temperatures the population of the $^4T_{2g}$ level increases and the intensity of the $^4T_{2g} \rightarrow {}^4A_{2g}$ emission increases while the intensity emission due to the $^2E_g \rightarrow {}^4A_{2g}$ transition decreases [37]. Because of the different values of Dq/*B* for YAB and GAB, different temperature dependent properties are expected.

Fig. 5 displays the temperature dependent emission spectra of the YAB:1%Cr phosphor. At lower temperatures the emission spectra exhibit only narrow lines due to the $^2E_g \rightarrow {}^4A_{2g}$ transition. In addition to that some weak vibronic side bands on the low-energy side of this line are detected. A considerable broadening of the bands starts to appear at 200 K and increases at higher temperatures. The broadening is due to thermal population of the $^4T_{2g}$ state and from the temperature dependence reflects the energy difference between the $^4T_{2g}$ and ^2E_g state.

In Fig. 6 normalized integrated emission intensity of the Cr^{3+} emission in the YAB:Cr and GAB:Cr phosphors are plotted as a function of temperature. In the low temperature regime a small increase in intensity is observed. Quenching does not occur until high temperatures with an onset around ~400 K in YAB:Cr^{3+} and 500 K for GAB:Cr^{3+}. These graphs confirm excellent thermal stability of the chromium luminescence in the borate host materials. The slight initial increase in emission intensity between 77 and 200 K is unexpected. It may be caused by an increase in the radiative decay rate due to thermal population of the $^4T_2$ level. A higher radiative transition probability combined with a constant non-radiative decay can explain the increase and has been observed before [38]. Alternatively, we cannot rule out that the comparison of integrated intensities between sharp line emission at low temperatures and band emission at higher temperatures is responsible for the increase. Comparison of intensities of sharp lines with that of broad bands is difficult and very small step sizes

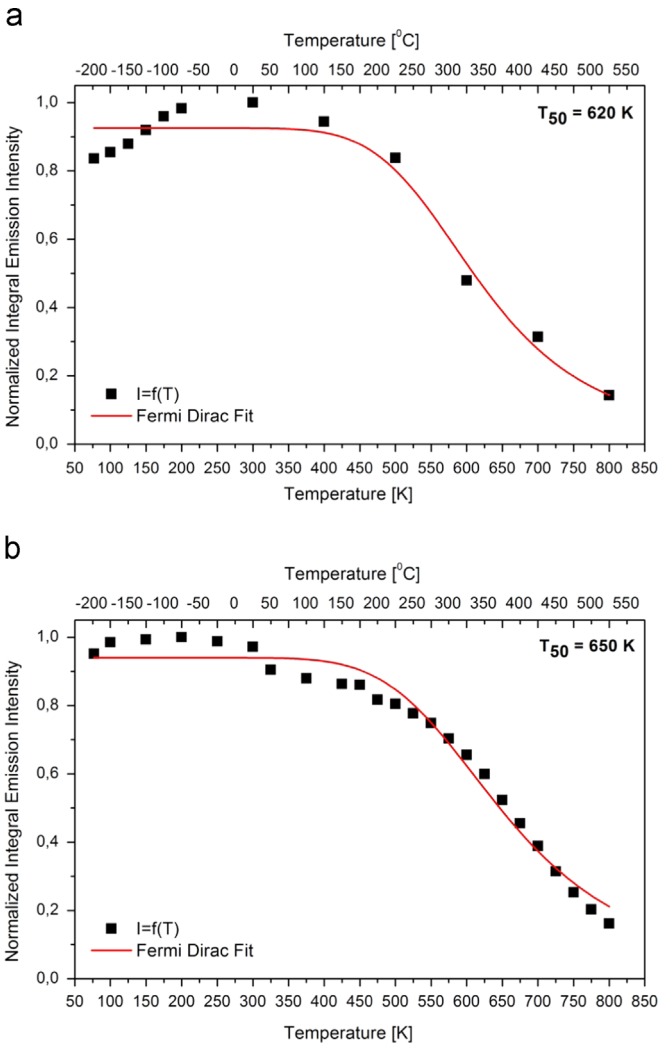

Fig. 6. Normalized integral emission intensity as a function of the temperature of YAB:1%Cr (a) and GAB:1%Cr (b).

are required to accurately determine integrated intensities of sharp lines. In addition, saturation effects in the peak of a sharp emission line may occur if for the same system settings broad bands are measured. Even though we have tried to eliminate an influence of these effects, it cannot be excluded that there is an error in the integrated intensities related to these effects. For the present paper the focus is on the high temperature regime. To determine the quenching temperature (T_{50}, the temperature when the phosphor loses 50% of its efficiency) a Fermi–Dirac fit was used. It was found that the quenching temperature for YAB and GAB phosphors are 620 and 650 K, respectively. Fermi–Dirac fitting enables us also to estimate the activation energy for the thermal quenching. The values are almost the same for YAB:1%Cr (0.41 eV) and GAB:1%Cr (0.40 eV). The higher thermal quenching temperature for GAB:Cr^{3+} shows that the thermally activated transition from the $^4T_{2g}$ level of Cr^{3+} to the $^4A_{2g}$ ground state requires thermal population of higher vibrational levels in the $^4T_{2g}$ excited state, reflecting a weaker electron phonon coupling [39].

In Fig. 7a closer look into temperature dependent emission spectra of GAB:1%Cr is shown by measuring higher resolution emission spectra in the region of the $^2E \rightarrow {}^4A_2$ transition. Three narrow emission lines are observed. Two lines are expected as the ^2E_g level splits into two sublevels $2\bar{A}$ (upper level) and $\bar{E}$ (lower level). The transitions $\bar{E} \rightarrow {}^4A_{2g}$ and $2\bar{A} \rightarrow {}^4A_{2g}$ are referred to the R_1 and R_2 lines, respectively [40]. The splitting of the doublet level

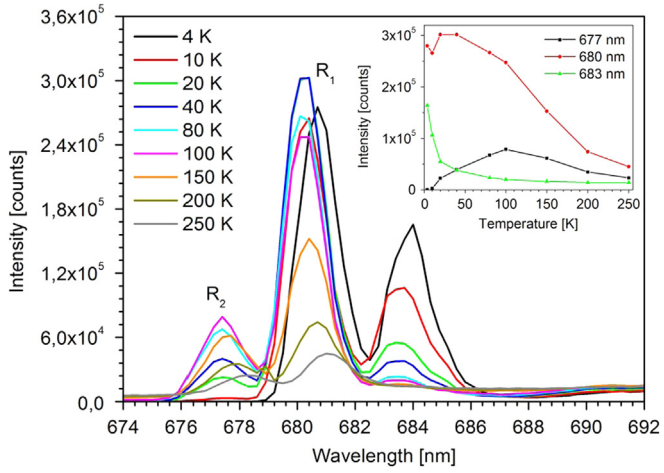

Fig. 7. Temperature dependence of high resolution emission spectra of GAB:1% Cr^{3+} in the range 4–250 K. The inset shows temperature dependence of the intensity of the three lines.

occurs, by the reason for the both lowering of site symmetry and the spin–orbit coupling [41].

The two emission lines at 680.5 and 677 nm show a temperature dependence that is typically observed for R_1 and R_2 emission lines. At 4 K only the R_1 line at 680.5 nm is observed similar to what was reported by Dominiak-Dzik et al. [42]. Increasing the temperature causes a decrease of the R_1-line intensity, whereas the intensity of R_2-line at 677 nm increases due to thermal population of the $2\bar{A}$ sublevel. Above 100 K, the intensities of the both R-lines decrease because of thermal population of the $^4T_2$ level giving rise to broad band emission as discussed above. Based on the spectral positions of the R_1 and R_2 line an energy difference of $\sim 60\ cm^{-1}$ is calculated for the $2\bar{A}$–$\bar{E}$ splitting which matches the 20–100 K temperature range where the rise of the R_2 line from the $2\bar{A}$ upper level is observed. The third emission line at 683 nm cannot be explained by a single Cr^{3+} center. The fact that two sharp emission lines are observed at 4 K, suggests that the 683 nm emission line is from a second Cr^{3+} site. We assign the 683 nm line to ^2E_g emission from exchange coupled Cr^{3+} pairs [43]. At elevated temperature also a red shift of R_1 and R_2 lines takes place. As the temperature is raised above 100 K, a shift to longer wavelengths is observed. The temperature induced redshift has also been observed for R-line emission for Cr^{3+} in other host lattices and is due to the phonon scattering processes [44].

Fig. 8 displays temperature dependent decay curves of ^2E_g emission of Cr^{3+} ions in YAB and GAB. Emission was monitored at 680.5 nm upon pulsed excitation at 420 nm. The decay curves are close to single exponential. At low temperatures a ms decay time is observed, typical of the spin- and parity-forbidden $^2E_g \rightarrow {}^4A_{2g}$ emission. The decrease in decay time at elevated temperatures is explained by thermal population of the $^4T_2$ level for the transition to the ground state is a spin-allowed (albeit still parity forbidden).

In Fig. 9 the temperature dependence of the decay times is shown for the Cr^{3+} emission in both host lattices. The temperature dependence is similar, with a slightly faster decrease of the decay time for GAB:Cr^{3+} between 77 and 150 K upon increasing the temperature. The emission arises from ^2E_g and $^4T_{2g}$ levels which are in thermal equilibrium levels resulting in a single lifetime which represents the population weighted average lifetime. The temperature dependence of the emission lifetime can be attributed to a change in the relative population of the two levels.

The lifetime of the spin-forbidden $^2E_g \rightarrow {}^4A_{2g}$ transition results from the mixing with $^4T_{2g}$ excited state through the spin–orbit interaction. Thus, the smaller energy separation between ^2E_g and $^4T_{2g}$ states, the greater mixing of these states and a higher

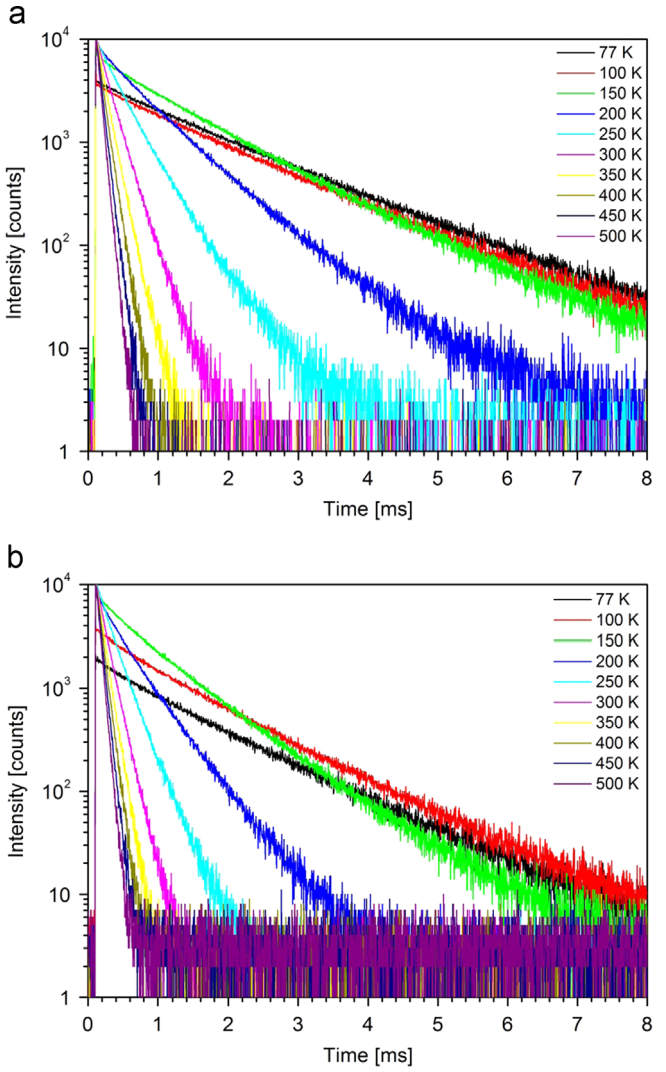

Fig. 8. Luminescence decay curves of YAB:1%Cr (a) and GAB:1%Cr (b) monitored at 680.5 nm under excitation at 420 nm.

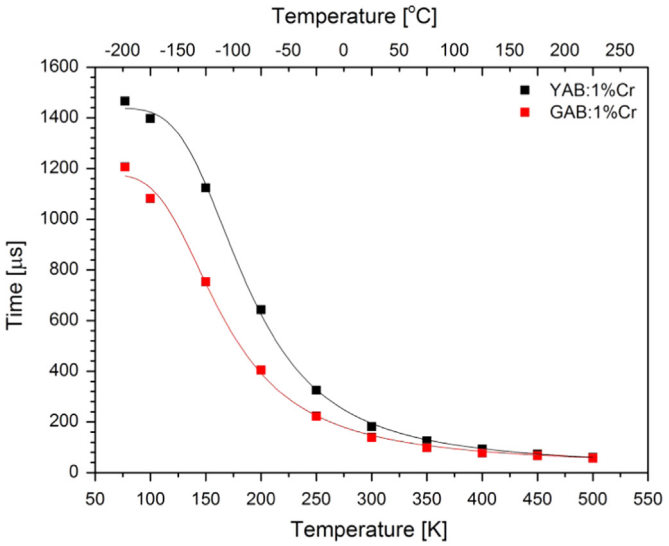

Fig. 9. Temperature dependent decay time of the R-line emission (680.5 nm) in YAB:1%Cr and GAB:1%Cr determined from single exponential fits of the decay curves displayed in Fig. 8. The drawn lines fit to a Boltzmann equation.

Table 3
Radiative lifetimes of ^2E_g ($\tau_2(0)$) and $^4T_{2g}$ (τ_4) states and zero phonon line $^4T_2$–^2E_g energy separation (ΔE_{ZPL}) of YAB:1%Cr^{3+} and GAB:1%Cr^{3+} derived from the Boltzmann fitting.

Parameter	$YAl_3(BO_3)_4$:1%Cr^{3+}	$GdAl_3(BO_3)_4$:1%Cr^{3+}
$\tau_2(0)$ [μs]	1438	1177
τ_4 [μs]	28	42
ΔE_{ZPL} [eV]	0.082	0.065

Table 4
Electron–phonon coupling parameters of GAB:1%Cr^{3+} and YAB:1%Cr^{3+} phosphors (FWHM-full width at half maximum, $\Delta E = E(^4A_{2g} \rightarrow ^4T_{2g}) - E(^4T_{2g} \rightarrow ^4A_{2g})$, S-Huang–Rhys parameter, $\hbar\omega$-effective phonon energy).

Parameter	$YAl_3(BO_3)_4$:1%Cr^{3+}	$GdAl_3(BO_3)_4$:1%Cr^{3+}
FWHM	2011 cm^{-1}	2155 cm^{-1}
ΔE	2862 cm^{-1}	3136 cm^{-1}
S	5.93	5.37
$\hbar\omega$	263 cm^{-1}	309 cm^{-1}

probability of the $^2E_g \rightarrow ^4A_{2g}$ transition (i.e. shorter emission lifetime) can be expected.

The dependence of the R-line luminescence lifetime (τ) can be described by the Boltzmann equation $1/\tau 2(T) = 1/\tau_2(0) + 3/\tau_4 \cdot \exp(-\Delta E/kT)$, where ΔE is the zero phonon line $^4T_{2g}$–^2E_g energy separation, k is the Boltzmann constant, τ_4 and $\tau_2(0)$ are the radiative lifetimes of $^4T_{2g}$ and ^2E_g states, respectively [45]. The best fit of the Boltzmann equation to the data is displayed as a solid line in Fig. 9. and the obtained fitting parameters are collected in Table 3.

For YAB and GAB doped Cr^{3+} a significant reduction in lifetime with increasing temperature can be observed (Fig. 9). This phenomenon occurs because of the much smaller decay rate of the $^2E_g \rightarrow ^4A_{2g}$ transition than the $^4T_{2g} \rightarrow ^4A_{2g}$ transition. Additionally, at low temperatures, where only ^2E_g level is occupied, the decay rate of $^2E_g \rightarrow ^4A_{2g}$ determines the lifetime. The reduction of the lifetime at higher temperatures results from the much higher decay rate of the $^4T_{2g} \rightarrow ^4A_{2g}$ transition, which appears due to the increased equilibrium population in the $^4T_{2g}$ state [46].

The mixture of $^4T_{2g}$ and ^2E_g states depends on the zero phonon line energy separation and determines the ratio of the doublet and quartet radiative lifetimes [36,47]. The values of ΔE_{ZPL} for YAB:1% Cr^{3+} and GAB:1%Cr^{3+} are 0.082 eV and 0.065 eV, respectively. The energy separation for YAB:1%Cr^{3+} is higher than for GAB:1%Cr^{3+} and is reflected by the longer doublet radiative decay time (Table 3). The quarter radiative lifetimes for both compounds are much shorter (30 μs for YAB:1%Cr^{3+} and 42 μs for GAB:1%Cr^{3+}) because the $^4T_{2g} \rightarrow ^4A_{2g}$ transition is spin allowed.

5. Electron–phonon coupling parameters

In order to study the interaction of the $^4T_2$–$^4A_2$ transition of the Cr^{3+} ions and the vibrations of the host lattice, the single-coordinate configuration model in harmonic approximation is used [48]. Two main parameters describing the electron–phonon coupling are the effective phonon energy $\hbar\omega$ and the Huang–Rhys parameter S. Both parameters can be determined from the spectroscopic data [34] and are included in Table 4.

The Huang–Rhys parameter S is larger for YAB ($S = 5.9$) than for GAB ($S = 5.4$) what indicates a stronger phonon coupling of Cr^{3+} ions in the $YAl_3(BO_3)_4$ host. The weaker electron–phonon coupling strength in GAB explains the higher quenching temperature for the Cr^{3+} emission in GAB in comparison with YAB.

6. Conclusions

The photoluminescence of Cr^{3+} in $YAl_3(BO_3)_4$ and $GdAl_3(BO_3)_4$ has been investigated between 4 and 800 K. At a low temperature ^2E_g emission dominates in both hosts. From the excitation and emission spectra the crystal field splitting and the Racah parameters B and C have been determined. The smaller value for B in GAB:1%Cr in comparison to YAB:1%Cr indicates a higher covalency (stronger nephelauxetic effect) for Cr^{3+} in GAB. Temperature dependent studies reveal a shift from ^2E_g to $^4T_{2g}$ emission upon raising the temperature and at room temperature the broad band IR emission from the $^4T_{2g}$ state dominates. The quenching temperature of the $^4T_{2g}$ emission is rather high, viz. 620 K (YAB:Cr) and 650 K (GAB:Cr), respectively. The higher quenching temperature of GAB:Cr is line with a weaker electron–phonon coupling strength, reflected by a smaller Huang–Rhys parameter S for Cr^{3+} in GAB. Efficient broad band NIR emission with little thermal quenching of Cr^{3+} is unusual and makes the efficiently NIR emitting YAB:Cr^{3+} and GAB:Cr^{3+} phosphors promising materials for application in phosphor converted (In,Ga)N LEDs for high power broad band NIR sources.

Acknowledgment

We gratefully acknowledge financial support from the Bundesdruckerei GmbH, Berlin, Germany.

Appendix A. Supplementary material

Supplementary data associated with this article can be found in the online version at http://dx.doi.org/10.1016/j.jlumin.2015.10.042.

References

[1] T.H. Maiman, R.H. Hoskins, I.J. D'Haenens, C.K. Asawa, V. Evtuhov, Phys. Rev. 123 (1961) 1151.
[2] M.Yu Sharonov, A.B. Bykov, P. Rojas, V. Petricevic, R.R. Alfano, Phys .Rev. B 72 (2005) 115111.
[3] J.C. Walling, O.G. Peterson, H.P. Jennsen, R.C. Morris, E.W. O'Dell, IEEE J. Quantum Electron QE-16 (1980) 1302.
[4] Z. Pan, Y.-Y. Lu, F. Liu, Nat. Mater. 11 (2012) 58.
[5] B. Atakan, C. Eckert, C. Pflitisch, Meas. Sci. Technol. 20 (2009) 075304.
[6] Z.Y. Zhang, K.T.V. Grattan, A.W. Palmer, Phys. Rev. B51 (1995) 2656.
[7] N. Basavaraju, S. Sharma, A. Bessière, B. Viana, D. Gourier, K.R. Priolkar, J. Phys. D.: Appl. Phys. 46 (2013) 375401.
[8] A. Bessière, S. Jacquart, K. Priolkar, A. Lecointre, B. Viana, D. Gourier, Opt. Express 19 (2011) 10131.
[9] A. Lakshmanan, Luminescence and Display Phosphors: Phenomena and Applications, Nova Science Publishers, New York, 2008.
[10] Y. Lee, C. Lee, C. Chen, J. IEEE, Quantum Electron 46 (2010) 1450.
[11] M.H. Bartl, K. Gatterer, E. Cavalli, A. Speghini, M. Bettinelli, Spectrochim. Acta A 57 (2001) 1981.
[12] X.X. Li, Y.H. Wang, Y. Hao, L.L. Wang, J. Electrochem. Soc. 153 (2006) G807.
[13] S.M. Borisov, K. Gatterer, B. Bitschnai, I. Klimant, J. Phys. Chem. C. 114 (2010) 9118.
[14] G. Wang, H.G. Gallagher, T.P.J. Han, B. Henderson, J. Cryst. Growth 163 (1996) 272.
[15] L.J.Q. Maia, C.R. Ferrari, V.R. Mastelaro, A.C. Hernandes, A. Ibanez, Solid State Sci. 10 (2008) 1835.
[16] J. He, H. Liang, D. Hou, S. Sun, Y. Huang, Z. Gao, Y. Tao, Mater .Chem. Phys. 132 (2012) 756.
[17] D. Wang, Q. Yin, Y. Li, M. Wang, J. Lumin. 97 (2002) 1.
[18] R.D. Shannon, Acta Cryst. A32 (1976) 751.
[19] J.S. Kim, J.S. Kim, H.L. Park, Solid State Commun. 131 (2004) 735.
[20] L.P. Sosman, R.J.M. da Fonseca, A. Dias Tavares Jr., R.B. Barthem, T. Abritta, J. Phys. Chem. Sol. 68 (2007) 22.
[21] M. Casalboni, V. Ciafardone, G. Giuli, B. Izzi, E. Paris, P. Prosposito, J. Phys.: Condens. Matter 8 (1996) 9059.
[22] R.G. Burns, Mineralogical Applications of Crystal Field Theory, second ed., Cambridge University Press, Cambridge, 1993.
[23] C.P. Poole Jr., J. Phys. Chem. Solids 25 (1964) 1169.

[24] G. Gauglitz, T. Vo-Dinh, Handbook of Spectroscopy, Wiley-VCH Verlag GmbH & Co. KGaA, Weinheim, 2003.
[25] M. Tanaka, Y. Katsuya, Y. Matsushita, J. Phys. Conf. Ser. 425 (2013) 132018.
[26] V.K. Pecharsky, P.Y. Zavalij, Fundamentals of Powder Diffraction and Structural Characterization of Materials, second ed., Springer, New York, 2009.
[27] V. Singh, R.P.S. Chakradhar, J.L. Rao, K. Al-Shamery, M. Haase, Y.-D. Jho, Appl. Phys. B 107 (2012) 489.
[28] J. García Solé, L.E. Bausá, D. Jaque, An Introduction to the Optical Spectroscopy of Inorganic Solids, John Wiley & Sons Ltd, England, 2005.
[29] M. Yamaga, B. Henderson, K.P. O'Donnell, C. Trager Cowan, A. Marshall, Appl. Phys. B 50 (1990) 425.
[30] H. Örücü, J. Collins, B. Di Bartolo, J. Appl. Phys. 108 (2010) 103101.
[31] Z. Nie, J. Zhang, X. Zhang, Y. Luo, S. Lu, X. Wang, J. Lumin. 119–120 (2006) 332.
[32] B. Henderson, G.F. Imbusch, Optical Spectroscopy of Inorganic Crystals, Oxford University Press, Oxford, 1989.
[33] G. Wang, T.P.J. Han, H.G. Gallagher, B. Henderson, Appl. Phys. Lett. 67 (1995) 3906.
[34] M.G. Brik, N.M. Avram, Z. Naturforsch. 59a (2004) 799.
[35] A. Trueba, P. Garcia-Fernandez, J.M. Garcia-Lastra, J.A. Aramburu, M.T. Barriuso, J. Phys. Chem. A 115 (2011) 1423.
[36] R. Martín-Rodríguez, R. Valiente, F. Rodríguez, M. Bettinelli, Nanotechnology 22 (2011) 265707.
[37] K.T.V. Grattan, Z.Y. Zhang, Fiber Optic Fluorescence Thermometry, Chapman & Hall, London, 1995.
[38] S.R. Rotman, Wide-Gap Luminescent Materials: Theory and Applications, Kluwer Academic Publishers, New York (1997), p. 23–27.
[39] A.H. Khalid, K. Kontis, Sensors 8 (2008) 5673.
[40] W. Koechner, Solid-State Laser Engineering, Sixth ed., Springer, New York, 2006.
[41] H. Orucu, G. Ozen, J. Collins, B. Di Bartolo, Opt. Mater, 31, (2009) 1065.
[42] G. Dominiak-Dzik, W. Ryba-Romanowski, M. Grinberg, E. Beregi, I. Kovacs, J. Phys.: Condens. Matter 14 (2002) 5229.
[43] N.M. Trindade, A. Tabata, R.M. Fernandes Scalvi, L. Vicente de Andrade Scalvi, Mater. Sci. Appl. 2 (2011) 284.
[44] W.A. Wall, J.T. Karpick, B. Di Bartolo, J. Phys. C.: Solid State Phys. 4 (1971) 3258.
[45] M. Grinberg, Phys. Status Solidi (a) 130 (1992) K189.
[46] S.M. Healy, C.J. Donnelly, T.J. Glynn, G.F. Imbusch, G.P. Morgan, J. Lumin. 46 (1990) 1.
[47] A.J. Wojtowicz, M. Grinberg, A. Lempicki, J. Lumin. 50 (1991) 231.
[48] M. Grinberg, I. Sokólska, S. Kück, W. Jaskólski, Phys. Rev. B 60 (1999) 959.